

## Multiple Comparison Procedures for Neuroimaging Genomewide Association Studies

Anonymous author

**SUMMARY:** Recent researches in neuroimaging have focused on assessing associations between genetic variants that are measured on a genomewide scale, and brain imaging phenotypes. A large number of works in the area apply massively univariate analyses on a genomewide basis to find single nucleotide polymorphisms that influence brain structure. In this paper, we propose using various dimensionality reduction methods on both brain structural MRI scans and genomic data, motivated by the Alzheimer's Disease Neuroimaging Initiative (ADNI) study. We also consider a new multiple testing adjustment method and compare it with two existing false discovery rate (FDR) adjustment methods. Based on the results from both simulation studies and the real data analysis, our proposed procedure is able to find the association between genetic variants and brain volume difference with increased power.

**KEY WORDS:**

Distance covariance; False discovery rate; Genomewide association studies; Local false discovery rate; Multivariate analysis; Neuroimaging analysis; Multiple comparison procedures.

## 1. Introduction

Advanced automated imaging techniques have allowed the assessment of genetic association of brain phenotypes for complex diseases, such as schizophrenia (Potkin et al., 2009), and Alzheimer’s disease (Furney et al., 2010). In this work we consider data from the Alzheimer’s Disease Neuroimaging Initiative (ADNI) project consisting of genetic variants encoded as single nucleotide polymorphisms (SNPs) across whole genome, and brain structure measured with tensor-based morphometry (TBM) based on brain structural magnetic resonance imaging (MRI) scans. TBM computes the volume of a local brain region in a given subjects’ MRI relative to an average template image based on healthy subjects. A signature of Alzheimer’s Disease (AD) is thinning of the cortical gray matter and increase of cerebral spinal fluid volume, in particular in the ventricles. Thus, TBM is sensitive to AD-related changes through decreases in volume (in cortex) and increases in volume (in ventricles). Stein et al. (2010b) conducted a voxelwide and genomewide study using TBM maps from each subject, where each voxel is evaluated with a regression at each SNP based on the SNP’s minor allele count, and using demographic variables as features with quantitative trait as responses. In their experiment, no significant loci were found after a false discovery rate with multiple testing adjustment at level 0.05. In a later study, Stein et al. (2010a) performed a genomewide search on two brain phenotypes (temporal lobe and hippocampal volume) based on the prior results and the literatures. To investigate the association, they collected an independent samples for each phenotype and performed adjusted regression analysis on the second population. Overall, two significantly associated SNPs were identified: *rs10845840*, located on chromosome 12 within an intron of the *GRIN2B* gene, and *rs2456930*, which is in an intergenic region of chromosome 15. Both SNPs were significantly associated with bilateral temporal lobe volume, while no significant SNPs was found to have associations with hippocampal phenotype.

When performing analysis using univariate approaches, multiple testing procedures should be employed as there are many statistical tests being considered simultaneously. The most commonly used approach for multiple testing correction is the Bonferroni correction, which controls the family-wise error rate (FWER). An alternative error quantity called false discovery rate (FDR) was proposed for the multiple comparisons problem by Benjamini and Hochberg (1995). Later, Storey (2002) and Storey (2003) defined the positive false discovery rate ( $p$ FDR), which is the conditional expectation of false positive findings given at least one positive identifications has occurred. He also provided a  $q$ -value algorithm to control the  $p$ FDR. Efron et al. (2001) defined a local false discovery rate (localfdr), a Bayesian version of FDR. For its estimation, they fit a mixture model to a Gaussian transformation of the inverse cumulative distribution of the  $p$ -values. To relate the frequentist and Bayesian versions of FDR, Efron et al. (2001), Efron and Tibshirani (2002), and Storey (2002) proved that the FDR controlled by the Benjamini and Hochberg procedure is equivalent to empirical Bayesian FDR given the rejection regions. Furthermore, Newton et al. (2004) proposed a hierarchical mixture of Gammas for determining localfdr and Muralidharan (2010) showed that the localfdr estimation controls  $FDR/pFDR$  over the entire exponential distribution family.

[Figure 1 about here.]

The previously published ADNI analyses were able to find associated SNPs or genes that are likely to be related to some specific voxels of the brain scans. However, neighboring structures of the brain were not being considered, and this spatial neighboring interaction could play an important role in associations with disease risk. In this work, this issue is addressed by combining the neighboring voxels into 119 regions based on the GSK CIC atlas (Figure 1) from Tziortzi et al. (2011), and then the interaction effects of 119 regions are measured by the distance covariance statistic (Székely et al., 2007), which allows for inference on the

relationship between a 119-dimensional multivariate phenotype and a single SNP predictor across the entire genome.

We propose two major contributions. First, we utilize distance covariance for the neuroimaging genomewide association study. This framework is able to establish the relationships between genomic variants and brain structural MRI, where brain imaging information is used as a multivariate response. Consequently, we are able to reduce the number of tests being done by considering a multivariate response variable, which results in more powerful inference compared to the approach from Stein et al. (2010b). Second, we propose a localfdr modeling algorithm which is to fit a two-component Gamma mixture model on the all test statistics for the multiple testing adjustment. One probabilistic output of this model is the localfdr. This leads to a decision-theoretic rule for selecting significant SNPs that is related to the approach of Newton et al. (2004). We also evaluate two existing methods for comparison in multiple testing setp. Based on our simulation studies, experiments show that the proposed method is able to control FDR even in situations when the data generating model does not match the mixture model. In addition, we also present the disease status classification and the corresponding pathway analysis based on our significant SNP findings. The significant SNPs selected from our procedures achieved promising prediction accuracy in the disease classification analysis (Section 4.3) and provide signal enrichment functions through pathway to AD (Table 6) from the Database for Annotation, Visualization and Integrated Discovery (DAVID v6,7).

The structure of this paper is as follows: Section 2 reviews the details of ADNI data. We then introduce our methods of distance covariance statistic and multiple testing adjustment procedure in Section 3. In Section 4, we present the results by applying our method and evaluate its performance comparing to two existing methods on both simulated data and ADNI dataset. Finally, some discussion concludes Section 5.

## 2. Materials

Data used in the preparation of this article were obtained from the ADNI study. The SNPs data and the TBM data from the ADNI study are processed by Paul Thompson's group, which are the same as those used in the previous studies (Stein et al., 2010b). Here we introduce the ADNI study and then describe all the genetic data and imaging data preprocessing for completeness.

### 2.1 ADNI study

The ADNI project was launched in 2003 by the National Institute on Aging (NIA), the National Institute of Biomedical Imaging and Bioengineering (NIBIB), the Food and Drug Administration (FDA), private pharmaceutical companies and non-profit organizations, as a 60 million, 5-year public-private partnership. The primary goal of ADNI has been to test whether serial MRI, positron emission tomography (PET), other biological markers, and clinical and neuropsychological assessment can be combined to measure the progression of mild cognitive impairment (MCI) and early AD. For up-to-date information, see [www.adni-info.org](http://www.adni-info.org). The ADNI dataset released 852 subjects, but we discarded 111 of the subjects because 741 samples are unrelated Caucasian subjects identified by self-report ethnicity and verified by multi-dimensional scaling (MDS) analysis (Stein et al., 2010a). Volumetric brain differences were assessed in 206 normal older controls, 358 MCI subjects, and 177 AD patients.

### 2.2 Genetic analysis

ADNI released 620,901 SNPs using the Illumina 610 Quad array. SNPs that did not fulfil the following quality control criteria were excluded: genotype call rate smaller than 95%, significant deviation from Hardy-Weinberg equilibrium where  $p$ -values  $< 5.7 \times 10^{-7}$ , allele

frequency smaller than 0.10, and a quality control score of smaller than 0.15. After applying this list of quality criteria, we obtain a total of 448,244 SNPs for the analysis.

### 2.3 Brain MRI scans

Three-dimensional T1-weighted baseline MRI scans were analyzed using TBM, which is a method for representing structural differences between local brain regions and a template brain into a deformation field (Frackowiak et al., 2004). The deformation field contains the information on relative positions of different brain scans, while the local shapes (such as volumes, lengths and areas) are encoded in the Jacobian matrix. Therefore, TBM can be used to recognize the local shape of brain differences. The MRI scans were acquired at 58 different ADNI sites, all with 1.5T MRI scanners using a sagittal 3D MP-RAGE sequence for across-site consistency (Jack et al., 2008). All images were calibrated with phantom-based geometric corrections. The scans were linearly registered with 9 parameters to the International Consortium for Brain Image template (Mazziotta et al., 2001) to adjust for differences in brain position and scaling. Each subject's MRI scan was registered against a template scan which is the average of all the healthy subjects (minimal deformation template), using a non-linear inverse-consistent elastic intensity-based registration method (Leow et al., 2005). Furthermore, voxel size variation from registration is represented as the voxel intensity, which is the volumetric difference between the subject and the reference template, calculated from taking the determinant of the Jacobian matrix of the deformation fields. Finally, each brain scan volume is down-sampled to 1/4 of its original size (using trilinear interpolation to  $4 \times 4 \times 4 \text{ mm}^3$ ), which results into 31,622 total voxels per scan for faster experimental processing. As in Stein et al. (2010b)'s work, we use the volumetric difference representation of MRI scans as a quantitative measure of brain tissue volume difference.

We mostly focused on genomewide associations with brain volume differences using regions

of interests (ROIs). This allows for information on local neighborhoods of voxels to be pooled. In order to conduct the experiment using 119 ROIs, we extracted voxels from each brain region, and computed the average Jacobian scores (per region) that make up the 119 different brain regions from the GSK CIC Atlas as shown in Figure 1, which is based on the Harvard-Oxford atlas with a 6-level hierarchy. To extract the corresponding voxels from each brain region in the atlas, we used the FLIRT linear registration tool from FSL (Jenkinson and Smith (2001), Jenkinson et al. (2002), Smith et al. (2004), and Woolrich et al. (2009)) in order to register the brain atlas to our template scan. This allows us to extract voxels of different brain regions from the subject's scan and the registered atlas by direct comparison. We then used the average per-region Jacobian scores from each of the 119 ROIs as the response into genomewide association, and denoted it as the region-wide study.

### 3. Methods

#### 3.1 Distance covariance

We now briefly discuss the distance covariance statistic that was proposed by Székely et al. (2007) and Székely and Rizzo (2009). Let  $\phi_X$  and  $\phi_Y$  be the characteristic functions of  $X$  and  $Y$ , where  $X \in \mathbb{R}^p$  and  $Y \in \mathbb{R}^q$  are two random vectors from two arbitrary dimensions  $p$  and  $q$ , respectively. The distance covariance  $\text{dCov}^2(X, Y)$  between random vectors  $X$  and  $Y$  is a non-negative value with finite first moments:

$$\begin{aligned} \text{dCov}^2(X, Y) &= \|\phi_{X,Y}(x, y) - \phi_X(x)\phi_Y(y)\|^2 \\ &= \int_{\mathbb{R}^{p+q}} |\phi_{X,Y}(x, y) - \phi_X(x)\phi_Y(y)|^2 w(x, y) \, dx dy, \end{aligned} \tag{1}$$

where  $w(x, y)$  is a positive weight function for which the integral in Eq. 1 exists.

The sample distance covariance estimator from Székely et al. (2007) and Székely and Rizzo (2009) requires that there be no missing values among observations  $X_i$ 's and  $Y_j$ 's for  $i, j =$

$1, \dots, n$ . Here, we propose a modified version by assuming the data is missing completely at random (Rubin, 1976), to relax the non-missing values requirement of sample distance covariance. The main idea of this modification is to save additional computational cost when modeling the missing values. Here,  $\delta$  is defined as an indicator which indicates if a variable is missing or present:

$$\delta_k = \begin{cases} 1, & \text{if variable } k \text{ is present} \\ 0, & \text{if variable } k \text{ is missing} \end{cases}. \quad (2)$$

By adjusted the indicator  $\delta$  for observations  $X_i$ 's and  $Y_j$ 's, it basically puts the larger weights on observations with no missing values and zero weight on observations with missing values. Therefore, the modified sample distance dependence statistics according to Székely et al. (2007) are defined as:

$$A'_{ij} = a'_{ij} - \bar{a}'_{i.} - \bar{a}'_{.j} + \bar{a}'_{..}; \quad (3)$$

where

$$a'_{ij} = \frac{|X_i - X_j|_p \delta_i \delta_j}{P(\delta_i = 1)P(\delta_j = 1)}, \quad \bar{a}'_{i.} = \frac{1}{n} \sum_j^n a'_{ij}, \quad \bar{a}'_{.j} = \frac{1}{n} \sum_i^n a'_{ij}, \quad \text{and} \quad \bar{a}'_{..} = \frac{1}{n^2} \sum_{i,j}^n a'_{ij}.$$

Similarly, we define

$$b'_{ij} = \frac{|Y_i - Y_j|_q \delta_i \delta_j}{P(\delta_i = 1)P(\delta_j = 1)}$$

and  $B'_{ij} = b'_{ij} - \bar{b}'_{i.} - \bar{b}'_{.j} + \bar{b}'_{..}$  for  $i, j = 1, \dots, n$ .

The modified sample distance covariance  $\widetilde{\text{dCov}}_n^2(X, Y)$  is then given by  $\widetilde{\text{dCov}}_n^2(X, Y) = n^{-2} \sum_{i,j=1}^n A'_{ij} B'_{ij}$ . Having proposed a modified empirical distance covariance for situations when there are missing values, we now wish to study its asymptotic property under the independent assumption. The expectation of  $a'_{ij}$  in Eq. 3 is:

$$\begin{aligned} E(a'_{ij}) &= E \left\{ \frac{|X_i - X_j|_p \delta_i \delta_j}{p(\delta_i = 1)p(\delta_j = 1)} \right\} \\ &= E(|X_i - X_j|_p) \end{aligned}$$

and similarly,  $E(b'_{ij}) = E(|Y_i - Y_j|_q)$ . Arguing as in Székely et al. (2007), we have that if



$E|X|_p < \infty$  and  $E|Y|_q < \infty$ , then  $\widetilde{\text{dCov}}_n \rightarrow_{a.s} \text{dCov}$  under the null hypothesis. Similarly,  $n \times \widetilde{\text{dCov}}_n^2 / T'_2$  converges in distribution to  $Q$ , where  $T'_2 = n^{-2} \sum_{i,j=1}^n a'_{ij} n^{-2} \sum_{i,j=1}^n b'_{ij}$  and  $Q$  is a positive semidefinite quadratic form of centered Gaussian random variables with  $E(Q) = 1$ . In terms of obtaining a p-value based on the distribution of  $Q$ , we apply a Gamma approximation for inference for the distance covariance statistics (Gretton et al., 2008), which is discussed in next section.

### 3.2 Multiple testing procedure

We now review the multiple testing problem and define FDR. Assuming there are  $m$  tests for the study, and the goal is to identify significant SNP variants given a certain alpha level. Table 1 shows the possible outcomes of conducting  $m$  tests simultaneously, for which the null hypothesis is true in  $m_0$  of them. Of the  $m$  tests of hypotheses,  $W$  hypotheses are failed to be rejected, and  $R$  rejected the null hypothesis.

[Table 1 about here.]

Benjamini and Hochberg (1995) introduced a new measure called FDR, defined as:

$$FDR = E \left[ \frac{V}{R} | R > 0 \right] P(R > 0) \quad (4)$$

Storey (2002) and Storey (2003) proposed another measure, positive false discovery rate ( $p\text{FDR}$ ), which is the expected false-positive rate conditionally on positive finding ( $P(R = 0) > 0$ ). The  $p\text{FDR}$  takes the following form:

$$p\text{FDR} = E \left[ \frac{V}{R} | R > 0 \right] \quad (5)$$

Our aim is to control  $p\text{FDR}$ , and three algorithms are presented in this section.

The first algorithm is the  $q$ -value algorithm, which was presented by Storey (2002), who introduced  $p\text{FDR}$ . The requirement for  $q$ -value is having prior knowledge of the null distribution of the test, such that the  $p$ -values can be computed under the null density. In the case of distance covariance, Gretton et al. (2008) proposed to fit a Gamma distribution as

the null density, where the parameters are

$$\alpha = \frac{E^2(dCov_n)}{Var(dCov_n)}, \quad \beta = \frac{Var(dCov_n)}{E(dCov_n)}. \quad (6)$$

Hence, the parameter for  $\alpha$  and  $\beta$  in Eq. 6 can be estimated by the distance covariance statistics, and the  $p$ -values were able to be collected from a Gamma fitting for  $q$ -value method. The algorithm for  $q$ -value method is as follows: First, for each  $T_i$ , we compute the  $p$ -value  $p_i$  under a Gamma approximation. Next, we compute  $q$ -values  $q_1, \dots, q_m$  for each test using the method of Storey (2003). Defining  $\tilde{q} = \arg \max_i \{q_i \leq \alpha\}$ , we reject all tests with  $q_i \leq \tilde{q}$ . Storey (2002) and Storey (2003) have showed that the  $q$ -value algorithm (Algorithm 1) controls FDR under the desired  $\alpha$  level. Note that step 2 of the above algorithm is computed using the publicly available R-package **qvalue**.

The second algorithm is the local false discovery rate from Efron et al. (2001), which is related to a Bayesian interpretation for  $p$ FDR of Storey (2002) and Storey (2003). In Efron et al. (2001)'s work, the null distribution is assumed either known or collected by permutations. Here, we chose to use a Gamma approximation with empirical estimations of E.q. (6) as the null density candidate for the distance covariance statistics. The following algorithm displays the summary of Efron et al. (2001)'s work.

**Algorithm 2:**

Input:  $m$  hypotheses with statistics  $T_1, \dots, T_m$ .

1. For each  $T_i$ , compute the  $p$ -values  $p_i$  under the Gamma approximation.
2. For each  $p_i$ ,  $z_i = \Phi(p_i)$ , for all  $i$ .
3. Estimate the parameters using a Gaussian mixture model (GMM) to the  $z_i$ 's.
4. Compute `localfdr` as defined in Efron et al. (2001).
5.  $\widehat{pFDR}(z)$  is the conditional expectation of  $\widehat{localfdr}(z)$  given  $z \in \Gamma$ .
6. Define  $\tilde{z} = \arg \max_z \{\widehat{pFDR}(z) \leq \alpha\}$ , and reject all tests with  $z_i$  in rejection region. In theory, this gives an  $p$ FDR no greater than  $\alpha$ .

We now propose a new algorithm (denoted as *localfdr* modeling) based on the distance covariance described in Section 3.1 for multiple testing adjustment. The traditional multiple correction methods are based on  $p$ -values (e.g., algorithm 1 and 2), while our proposed method models the test statistics directly. The *localfdr* modeling algorithm is similar to algorithm 2, where it simply skips step (2) of algorithm 2. This rule is similar to one proposed by Newton et al. (2004) in a different genomics setting, where more powerful inference can be obtained by not mapping the test statistics from  $t_i$ 's to  $z_i$ 's.

**Algorithm 3 (*localfdr* modeling algorithm):**

Input:  $m$  hypotheses with statistics  $T_1, \dots, T_m$ .

1. Fit a two-component mixture of Gammas on all  $T_i$ 's.
2. Estimate the parameters using EM algorithm.
3. Compute *localfdr*.
4.  $\widehat{pFDR}(t)$  is the conditional expectation of  $\widehat{localfdr}(t)$  given  $t \in \Gamma$ .
5. Define  $\tilde{t} = \arg \max_t \{\widehat{pFDR}(t) \leq \alpha\}$ , and reject all tests with  $t_i \geq \tilde{t}$ .

#### 4. Simulation study and real data analysis

We implemented and analyzed our numerical experiments in R, Matlab and C, where Matlab was used to compute the distance covariance statistics. In addition, we evaluated the performance of Stein et al. (2010b)'s work by a C implementation. The simple linear regression statistics were calculated across the whole genome, the procedure was split for parallel computing across 256 cluster nodes. After collecting all the statistics for the correlation test, the R packages *qvalue*, *mixfdr*, and *mixtools* were applied in our second phase of analysis. All the analyses in C, Matlab and R were accomplished by using the university computing cluster, which consists of 8 servers with 4 Xenon E7-8837 processors, 8 cores each for a total of 256 cores and 96 GB of memory.

#### 4.1 Simulation Design

To evaluate the performances of the methods described in Section 3, we simulated the data to assess the FDR and power estimates by controlling  $\alpha$  at desired levels. The setting of the simulation studies was to mimic the structure of the genotypes and the phenotypes of the ADNI study. We considered two type of correlations (i.e., the pure linear correlation, and the mixed linear and non-linear correlations) and the impact of univariate and multivariate effects into three simulation settings. For each setting, the samples were generated from two populations, i.e., the null population and alternative. In this first case, we generated 50 pairs samples. Each pair consisted of a single genotype and a phenotype, and followed a bivariate Normal distribution, where the correlation coefficient  $\rho$  was 0.8 under the alternative and  $\rho$  equalled to zero under the null. The second and the third case, the sample size became 100, and the univariate genotype was generated from  $N(0, 1)$ , but the dimensions of phenotype were enlarged to 30. The  $100 \times 30$  phenotype data formed the mixed association effects between phenotypes and the genotypes under the alternative, where the mixed associations were linear, exponential and quadratic transformations (i.e., 10 duplicated copy of 100 genotypes, 10 exponential transformation of 100 genotypes, and 10 quadratic form of 100 genotypes). For the null population, the single genotype again was generated from  $N(0, 1)$  and the 30-dimensional phenotypes followed a multivariate Normal with mean 0 and covariance matrix  $\Sigma$ , where  $\Sigma$  was the independent in the second simulation design and positive dependent (diagonal terms are one and off diagonal terms are 0.5) on third case. The ratio between the null population and the alternative population for each run was 1:19, and 1000 runs were repeated for each setting to assess the FDR and power performances.

#### 4.2 Simulation Results

Three FDR procedures were presented in Section 3.2, which are summarized as follows:

Alg. 1:  $p$ -values (from Gamma approximation) +  $q$ -values method (Storey, 2003)

Alg. 2:  $p$ -values (from Gamma approximation) + the localfdr method (Efron and Tibshirani, 2002)

Alg. 3 (localfdr modeling):  $dCov_n$  + the localfdr method (Efron and Tibshirani, 2002)

Three simulations were designed from Section 4.1 for evaluating the performances of the three algorithms above. Before we discussed FDR and power estimates of the three algorithms, first we performed the size analysis to evaluate if a Gamma approximation (Gretton et al., 2008) is the proper null density for algorithm 1 and 2. 1000 (genotype v.s. phenotype) paired samples were generated all from the null population per single run under each of the three simulations, and 50 runs were repeated to calculate the size. Table 2 reports the size estimates according to nominal values from 0.1, 0.2,...,1, and they are very close to each other for all three simulations. Therefore, we can conclude that the Gamma approximation is an appropriate null distribution for the distance covariance statistic.

[Table 2 about here.]

[Table 3 about here.]

Table 3 shows the average FDR, the average power, and their standard error at nominal  $\alpha$  levels 0.05, 0.1, 0.15 and 0.2 for the three simulations. The results show that the average FDR are all close or lower to the desired  $\alpha$  values. The power performances of algorithm 2 and 3 outperform algorithm 1 in all the  $\alpha$  values, this implies the algorithms utilized the localfdr method result in powerful inference. In addition, the average estimated power of simulation 3 is smaller but close to the power of simulation 2 at each level. This shows the results of all FDR adjusted algorithms are slightly affected by the noise of the dependent covariance structure between voxel features, but the overall performances are quite robust. Furthermore, the results of algorithm 2 and 3 are similar in our simulation studies, and this suggests that algorithm 3 controls FDR.

### 4.3 Application to ADNI data sets

We also evaluated the three algorithms using the ADNI dataset. For each algorithm, we set the independent variable as a single SNP across the whole genome (448,244 SNPs), and the response variable was the average value from each of the 119 ROIs based on the GSK CIC Atlas (in Section 2.3). In addition to the three algorithms described in Section 3.2, we also re-implemented the procedure in Stein et al. (2010b)'s work, where they considered simple linear regression (slr) as the association test between each single SNP and each single brain region, which are  $448,244 \times 119$  tests. For this method, we selected the brain region with the highest  $p$ -value at each SNP, used the localfdr to perform multiple testing adjustment, and denoted this procedure as algorithm 4 (slr + the localfdr method).

[Table 4 about here.]

[Table 5 about here.]

Table 4 shows the number of significant SNPs controlled by the  $\alpha$  values from each algorithm. Notice that there are 1180 significant SNPs at  $\alpha$  level 0.5 in algorithm 4 (Stein et al., 2010b), while algorithm 2 and 3 result in more than 20,000 findings, with algorithm 1 having slightly above 5,000 SNPs at the same  $\alpha$  level. In order to compare the inference information of the significant SNPs in Table 4, the top 1180 SNPs were selected from each of the algorithm as the input variables for disease status classification. Specifically, we focused on binary disease status classification (206 normal patients against 177 AD's) due to the fact that AD is the definitive form of the illness with much higher severity than MCI. We used LIBSVM (Chang and Lin, 2011) for binary classification with leave-one-out to compute the prediction accuracy. The majority count is 53.79%, and the prediction accuracy of top 1180 SNPs from algorithm 1, 2 and 3 is 57.44%, this is because the top 1180 SNPs from the three algorithms are exactly the same. The prediction accuracy of algorithm 4 is the same as the majority count. In addition, the algorithm 1, 2 and 3 at  $\alpha$  level 0.05 found 5,388, 27,965, and

23,128 significant SNPs (Table 4); these SNPs yield 57.96%, 62.14%, and 62.40% prediction accuracies, respectively.

The functional annotation clustering analysis was done using DAVID v6.7 (Dennis Jr et al., 2003). Table 5 lists the top 8 clusters enrichment scores and the total enrichment scores. Since the top 1180 SNPs from algorithm 1, 2 and 3 are the same, therefore the enrichment scores from these three algorithms are identical and the total scores are 10.257, which is greater than the total enrichment scores of 5.739 from algorithm 4. This implies that algorithm 4 (Stein et al., 2010b) yields less significant findings even with a higher nominal  $\alpha$  level, and the 1180 SNPs contain less information in both disease status classification and functional annotation clustering analysis.

In addition to the enrichment scores of the functional annotation clustering analysis, Table 6 lists top 5 enriched terms based on the significant SNPs identified by algorithm 2 and 3 at level 0.05 of Table 4. These promising results imply that these enriched terms may point out the important pathways to Alzheimer’s disease. Finally, 4 categories out of top 5 enriched term in Table 6 are the same from the enriched terms of algorithm 2 and 3, and this confirms the findings from the simulation study that algorithm 2 and algorithm 3 have similar performances.

[Table 6 about here.]

## 5. Discussion and Conclusion

In this work, we have developed three multivariate multiple testing procedures for neuroimaging genomics study using the ADNI dataset. The proposed methods are able to identify the dependencies between the SNP variants and the brain volume differences, and utilize voxel neighborhood information from the brain regions at the same time. We also proposed a novel localfdr modeling strategy and compared the performances with two existing FDR

adjustment methods. From both the simulation study and real data analysis,  $p$ -values from Gamma approximation with the localfdr method (algorithm 2), and distance covariance with the localfdr method (algorithm 3) were able to control FDR at the proper levels. In the real data application, the significant SNPs found by distance covariance contained more information than simple linear regression (Stein et al., 2010b) in both disease status classification, and function annotation clustering analysis. This is because the simple linear regression only captured the linear relationship between SNPs and brain MRI scans, while the distance covariance was able to model non-linear associations.

In addition to the distance covariance statistic extension of Székely et al. (2007) to account for missing data, another option to deal with the missing values is to impute the genotypes by using genotype imputation tools. We used PLINK to impute the missing values of ANDI study as it is computationally more efficient (Li et al., 2009). The imputed algorithm of PLINK uses the standard E-M algorithm and performs probabilistic estimation for each allele combination based on the relatively small regions of genome for each individual (Purcell et al., 2007). Based on the results of our PLINK imputation, the rate of missing data decreased by only 0.3%. Therefore, we work with the original dataset and leave imputation algorithms with distance covariance for future investigation.

There remains many open questions that could lead to important further developments. We utilized the distance covariance to measure the relationship between genetic variants and differences in brain volumes in the first stage; this representation can be applied to capture the non-linear dependencies between two sets of vectors with arbitrary dimensions, but it also suffers possible biases when the number of dimensionality is much greater than the sample size (Cope, 2009). Therefore, we placed more emphasis on the region-wide study in this work, and we plan to study different regularization approaches to the dependency measure, in order to reduce this bias in our next steps. Finally, it would also be desirable to



develop distance covariance-type measures that explicitly incorporate the distance nature of the SNP data.

#### REFERENCES

- Benjamini, Y. and Hochberg, Y. (1995). Controlling the false discovery rate: a practical and powerful approach to multiple testing. *Journal of the Royal Statistical Society. Series B (Methodological)* pages 289–300.
- Chang, C.-C. and Lin, C.-J. (2011). Libsvm: a library for support vector machines. *ACM Transactions on Intelligent Systems and Technology (TIST)* **2**, 27.
- Cope, L. (2009). Discussion of: brownian distance covariance. *The Annals of Applied Statistics* **3**, 1279–1281.
- Dennis Jr, G., Sherman, B. T., Hosack, D. A., Yang, J., Gao, W., Lane, H. C., Lempicki, R. A., et al. (2003). David: database for annotation, visualization, and integrated discovery. *Genome Biol* **4**, P3.
- Efron, B. and Tibshirani, R. (2002). Empirical bayes methods and false discovery rates for microarrays. *Genetic epidemiology* **23**, 70–86.
- Efron, B., Tibshirani, R., Storey, J. D., and Tusher, V. (2001). Empirical bayes analysis of a microarray experiment. *Journal of the American statistical association* **96**, 1151–1160.
- Frackowiak, R. S., Friston, K. J., Frith, C. D., Dolan, R. J., Price, C. J., Zeki, S., Ashburner, J. T., and Penny, W. D. (2004). *Human brain function*. Academic Press.
- Furney, S. et al. (2010). Genome-wide association with mri atrophy measures as a quantitative trait locus for alzheimer’s disease. *Molecular psychiatry* **16**, 1130–1138.
- Gretton, A., Fukumizu, K., Teo, C. H., Song, L., Schölkopf, B., and Smola, A. J. (2008). A kernel statistical test of independence.
- Jack, C. R. et al. (2008). The alzheimer’s disease neuroimaging initiative (adni): Mri methods. *Journal of Magnetic Resonance Imaging* **27**, 685–691.

- Jenkinson, M., Bannister, P., Brady, M., and Smith, S. (2002). Improved optimization for the robust and accurate linear registration and motion correction of brain images. *Neuroimage* **17**, 825–841.
- Jenkinson, M. and Smith, S. (2001). A global optimisation method for robust affine registration of brain images. *Medical image analysis* **5**, 143–156.
- Leow, A. et al. (2005). Inverse consistent mapping in 3d deformable image registration: its construction and statistical properties. In *Information Processing in Medical Imaging*, pages 493–503. Springer.
- Li, Y., Willer, C., Sanna, S., and Abecasis, G. (2009). Genotype imputation. *Annual review of genomics and human genetics* **10**, 387.
- Mazziotta, J. et al. (2001). A probabilistic atlas and reference system for the human brain: International consortium for brain mapping (icbm). *Philosophical Transactions of the Royal Society of London. Series B: Biological Sciences* **356**, 1293–1322.
- Muralidharan, O. (2010). An empirical bayes mixture method for effect size and false discovery rate estimation. *The Annals of Applied Statistics* **4**, 422–438.
- Newton, M. A., Noueir, A., Sarkar, D., and Ahlquist, P. (2004). Detecting differential gene expression with a semiparametric hierarchical mixture method. *Biostatistics* **5**, 155–176.
- Potkin, S. G. et al. (2009). A genome-wide association study of schizophrenia using brain activation as a quantitative phenotype. *Schizophrenia bulletin* **35**, 96–108.
- Purcell, S. et al. (2007). Plink: a tool set for whole-genome association and population-based linkage analyses. *The American Journal of Human Genetics* **81**, 559–575.
- Rubin, D. B. (1976). Inference and missing data. *Biometrika* **63**, 581–592.
- Smith, S. M. et al. (2004). Advances in functional and structural mr image analysis and implementation as fsl. *Neuroimage* **23**, S208–S219.
- Stein, J. L. et al. (2010a). Genome-wide analysis reveals novel genes influencing temporal

- lobe structure with relevance to neurodegeneration in alzheimer's disease. *Neuroimage* **51**, 542–554.
- Stein, J. L. et al. (2010b). Voxelwise genome-wide association study (vgwas). *Neuroimage* **53**, 1160–1174.
- Storey, J. D. (2002). A direct approach to false discovery rates. *Journal of the Royal Statistical Society: Series B (Statistical Methodology)* **64**, 479–498.
- Storey, J. D. (2003). The positive false discovery rate: A bayesian interpretation and the q-value. *Annals of Statistics* pages 2013–2035.
- Székely, G. J. and Rizzo, M. L. (2009). Brownian distance covariance. *The annals of applied statistics* pages 1236–1265.
- Székely, G. J., Rizzo, M. L., and Bakirov, N. K. (2007). Measuring and testing dependence by correlation of distances. *The Annals of Statistics* **35**, 2769–2794.
- Tziortzi, A. C. et al. (2011). Imaging dopamine receptors in humans with [<sup>11</sup>C]-(+)-phno: Dissection of d3 signal and anatomy. *Neuroimage* **54**, 264–277.
- Woolrich, M. W. et al. (2009). Bayesian analysis of neuroimaging data in fsl. *Neuroimage* **45**, S173–S186.

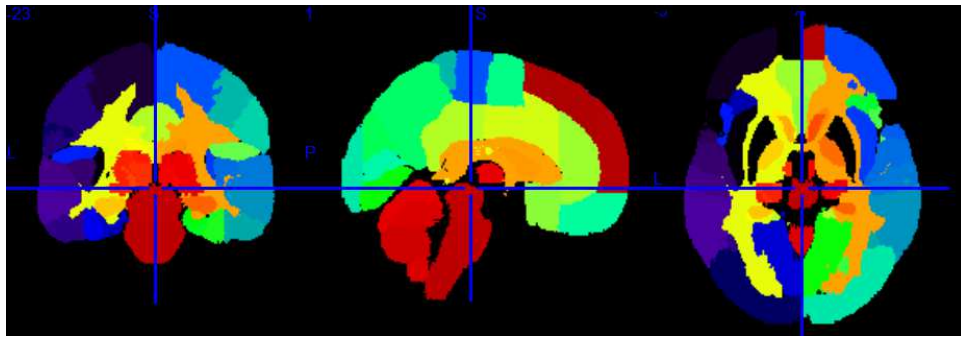


**Figure 1.** Plots showing from left to right: Coronal, Sagittal and Axial views of GSK CIC Atlas, color coded by the 119 region of interests.

**Table 1**  
Summary of the possible outcomes for simultaneously testing  $m$  hypotheses

	Accept null hypothesis	Reject null hypothesis	Total
Null true	$U$	$V$	$m_0$
Alternative true	$T$	$S$	$m_1$
	$W$	$R$	$m$

**Table 2**  
*Simulation results of the size analysis*

Size	Simulation 1	Simulation 2	Simulation 3
0.1	0.115	0.110	0.110
0.2	0.219	0.221	0.224
0.3	0.309	0.324	0.326
0.4	0.392	0.415	0.416
0.5	0.472	0.498	0.499
0.6	0.556	0.576	0.578
0.7	0.653	0.656	0.658
0.8	0.775	0.746	0.748
0.9	0.940	0.878	0.877
1.0	1.000	1.000	1.000

**Table 3**

*Simulation results of the average FDR estimates (with standard error) and the average power estimates (with standard error) of three algorithms described in Section 3.2; where Simulation 1 are the linear correlation, simulation 2 are the mixed correlations with independent covariance matrix, and simulation 3 are the mixed correlations with dependent covariance matrix in Section 4.1*

	$\alpha$	Alg. 1: $pvalue+qvalue$		Alg. 2: $pvalue + localfdr$		Alg. 3: $dCov_n + localfdr$	
		FDR (s.e.)	power (s.e.)	FDR (s.e.)	power (s.e.)	FDR (s.e.)	power (s.e.)
Simulation I	0.05	0.000 (0.000)	0.000 (0.000)	0.019 (0.026)	0.882 (0.065)	0.039 (0.121)	0.904 (0.068)
	0.10	0.006 (0.011)	0.691 (0.114)	0.063 (0.050)	0.964 (0.032)	0.080 (0.122)	0.965 (0.033)
	0.15	0.007 (0.012)	0.777 (0.142)	0.121 (0.068)	0.985 (0.019)	0.128 (0.127)	0.984 (0.020)
	0.20	0.028 (0.076)	0.900 (0.085)	0.186 (0.080)	0.993 (0.013)	0.184 (0.126)	0.990 (0.029)
Simulation II	0.05	0.000 (0.000)	0.000 (0.000)	0.020 (0.026)	0.801 (0.106)	0.035 (0.044)	0.882 (0.087)
	0.10	0.000 (0.000)	0.035 (0.026)	0.071 (0.051)	0.916 (0.085)	0.088 (0.061)	0.934 (0.038)
	0.15	0.002 (0.007)	0.467 (0.175)	0.134 (0.070)	0.950 (0.064)	0.150 (0.075)	0.959 (0.025)
	0.20	0.008 (0.016)	0.665 (0.159)	0.194 (0.080)	0.964 (0.048)	0.212 (0.082)	0.970 (0.016)
Simulation III	0.05	0.000 (0.000)	0.000 (0.000)	0.017 (0.024)	0.758 (0.095)	0.030 (0.033)	0.844 (0.066)
	0.10	0.000 (0.000)	0.020 (0.000)	0.064 (0.051)	0.899 (0.059)	0.084 (0.070)	0.918 (0.045)
	0.15	0.002 (0.007)	0.418 (0.179)	0.126 (0.070)	0.944 (0.036)	0.145 (0.091)	0.951 (0.029)
	0.20	0.004 (0.011)	0.572 (0.159)	0.194 (0.084)	0.963 (0.024)	0.208 (0.103)	0.965 (0.029)

**Table 4**  
*Comparison of ADNI dataset for the region-wide study.*

$\alpha$	Alg. 1	Alg. 2	Alg. 3	Alg. 4
0.05	5,388	27,965	23,128	0
0.10	8,447	34,659	29,288	18
0.15	11,041	39,875	34,261	38
0.20	13,804	44,604	38,794	95
0.30	19,299	53,716	47,535	275
0.40	25,537	63,449	56,853	612
0.50	448,073	75,030	68,365	1,180



**Table 5**

*Enrichment scores for each cluster from DAVID database. <sup>a</sup>: top 1180 SNPs were selected from 5388 SNPs in algorithm 1 at level 0.05; <sup>b</sup>: top 1180 SNPs were collected from 27965 SNPs in algorithm 2 at level 0.05; and <sup>c</sup>: top 1180 SNPs were collected from 23128 SNPs in algorithm 3 at level 0.05.*

Top 1180 SNPs from each algorithm in Table 4				
Annotation cluster	alg. 1 <sup>a</sup>	alg. 2 <sup>b</sup>	alg. 3 <sup>c</sup>	alg. 4
1	3.167	3.167	3.167	1.479
2	1.680	1.680	1.680	1.332
3	1.198	1.198	1.198	1.040
4	1.157	1.157	1.157	0.775
5	1.014	1.014	1.014	0.508
6	0.947	0.947	0.947	0.261
7	0.572	0.572	0.572	0.175
8	0.523	0.523	0.523	0.169
total	10.257	10.257	10.257	5.739

**Table 6***Top 5 enriched terms of 27,965 significant SNPs at 0.05 level from algorithm 2 in Table 4*

Annotation cluster	Top functions	Enrichment scores
1	Insoluble fraction , membrane fraction, and cell fraction	11.41
2	Vesicle, cytoplasmic membrane-bounded vesicle, cytoplasmic vesicle, and membrane-bounded vesicle	7.33
3	Regulation of apoptosis, programmed cell death, and cell death	6.85
4	ABC transporter-like, transmembrane region, conserved site ABC transporter integral membrane type 1, and defense mechanisms, ATPase, AAA+ type, core, AAA	5.78
5	Cellular homeostasis, cellular ion homeostasis, ion homeostasis, and cellular chemical homeostasis	5.69

*Top 5 enriched terms of 23,128 significant SNPs at 0.05 level from algorithm 3 in Table 4*

Annotation cluster	Top functions	Enrichment scores
1	Insoluble fraction , membrane fraction, and cell fraction	6.30
2	ABC transporter-like, transmembrane region, conserved site ABC transporter integral membrane type 1, and defense mechanisms, ATPase, AAA+ type, core, AAA	5.94
3	Regulation of apoptosis, programmed cell death, and cell death	5.48
4	Vesicle, cytoplasmic membrane-bounded vesicle, cytoplasmic vesicle, and membrane-bounded vesicle	4.85
5	ATPase activity hydrolase activity, P-P-bond-hydrolysis-driven transmembrane transporter activity and primary active transmembrane transporter activity	4.62